2005

An evaluation of ANSYS contact elements

Serhan Sezer
Louisiana State University and Agricultural and Mechanical College, ssezer1@lsu.edu

AN EVALUATION OF ANSYS CONTACT ELEMENTS

A Thesis

Submitted to the Graduate Faculty of the
Louisiana State University and
Agricultural and Mechanical College
in partial fulfillment of the
requirements for the degree of
Master of Science in Mechanical Engineering

in

The Department of Mechanical Engineering

by
Serhan Sezer
B.S., Yildiz Technical University, 2002
December 2005

ACKNOWLEDGEMENTS

I am thankful to my advisor, Dr. Glenn B. Sinclair for providing valuable advice and support throughout this research, to whom I will always be indebted. I would also like to thank Dr. Yitshak M. Ram and Dr. Su-Seng Pang for accepting to be part of my committee and their feedbacks on my thesis.

TABLE OF CONTENTS

ACKNOWLEDGEMENTS……..**ii**

LIST OF TABLES……**iv**

LIST OF FIGURES……**vii**

ABSTRACT……**viii**

1 INTRODUCTION..……**1**
- 1.1 Background and Motivation..……**1**
- 1.2 Basic Approach..……**2**
- 1.3 Outline of Remainder of Paper..……**3**

2 TEST PROBLEMS ……**4**
- 2.1 Contact Patch Test (Problem *P*) ……**4**
- 2.2 Hertzian Contact (Problem *H*)……....**6**
- 2.3 Steuerman Contact (Problem *S*).....**11**
- 2.4 Flat Punch Contact (Problem *F*).....**14**

3 FINITE ELEMENT ANALYSIS.....**18**

4 ASSESSMENT OF ELEMENT PERFORMANCE AND CONCLUSIONS…...**24**

5 FUTURE WORK…….....**30**

REFERENCES.....**31**

APPENDIX.....**32**

VITA……**44**

LIST OF TABLES

1 Element numbers in meshes for problems…….23

2a Accuracy and convergence of 4Q elements.....28

2b Accuracy and convergence of 8Q elements……...28

3a $\overline{\sigma_z}$ from 4Q elements.....32

3b $\overline{\sigma_z}$ from 8Q elements.....32

4a $\overline{\sigma_z}$ from surface-to-surface 4Q elements……...33

4b $\overline{\sigma_z}$ from surface-to-surface 8Q elements……...33

4c $\overline{\sigma_z}$ from node-to-surface elements…….33

5a $\overline{\sigma_z}$ from surface-to-surface 4Q elements……...34

5b $\overline{\sigma_z}$ from surface-to-surface 8Q elements……...34

5c $\overline{\sigma_z}$ from node-to-surface elements…….34

6a $\overline{\sigma_z}$ from surface-to-surface 4Q elements……...35

6b $\overline{\sigma_z}$ from surface-to-surface 8Q elements……...35

6c $\overline{\sigma_z}$ from node-to-surface elements…….35

7a $\overline{\sigma_c}$ from surface-to-surface 4Q elements……...36

7b $\overline{\sigma_c}$ from node-to-surface 4Q elements……...36

7c $\overline{\sigma_c}$ from surface-to-surface 8Q elements……...36

7d $\overline{\sigma_c}$ from node-to-surface 8Q elements……...36

8a $\overline{\sigma_h}$ from surface-to-surface 4Q elements……...37

8b $\overline{\sigma_h}$ from node-to-surface 4Q elements……...37

8c $\overline{\sigma_h}$ from surface-to-surface 8Q elements……...37

8d $\overline{\sigma_h}$ from node-to-surface 8Q elements……...37

9a $\overline{\sigma_c}$ from surface-to-surface 4Q elements……...38

9b $\overline{\sigma_c}$ from node-to-surface 4Q elements……...38

9c $\overline{\sigma_c}$ from surface-to-surface 8Q elements……...38

9d $\overline{\sigma_c}$ from node-to-surface 8Q elements……...38

10a $\overline{\sigma_c}$ from surface-to-surface 4Q elements……..39

10b $\overline{\sigma_c}$ from node-to-surface 4Q elements……..39

10c $\overline{\sigma_c}$ from surface-to-surface 8Q elements……..39

10d $\overline{\sigma_c}$ from node-to-surface 8Q elements……..39

11a $\overline{\sigma_c}$ from surface-to-surface 4Q elements……..40

11b $\overline{\sigma_c}$ from node-to-surface 4Q elements.....40

11c $\overline{\sigma_c}$ from surface-to-surface 8Q elements……..40

11d $\overline{\sigma_c}$ from node-to-surface 8Q elements……..40

12a $\overline{\sigma_c}$ from surface-to-surface 4Q elements……..41

12b $\overline{\sigma_c}$ from node-to-surface 4Q elements……..41

12c $\overline{\sigma_c}$ from surface-to-surface 8Q elements……..41

12d $\overline{\sigma_c}$ from node-to-surface 8Q elements……..41

13a $\overline{\sigma_c}^*$ from surface-to-surface 4Q elements…….42

13b $\overline{\sigma_c}^*$ from node-to-surface 4Q elements…….42

13c $\overline{\sigma_c}^*$ from surface-to-surface 8Q elements……...42

13d $\overline{\sigma_c}^*$ from node-to-surface 8Q elements…….42

14a $\overline{\sigma_c}^*$ from surface-to-surface 4Q elements…….43

14b $\overline{\sigma_c}^*$ from node-to-surface 4Q elements…….43

14c $\overline{\sigma_c}^*$ from surface-to-surface 8Q elements……...43

14d $\overline{\sigma_c}^*$ from node-to-surface 8Q elements…….43

LIST OF FIGURES

1 Dovetail blade attachment for a gas turbine engine……1

2a Test problem geometry and coordinates for contact patch tests.....5

2b Test problem geometry and coordinates for Hertzian contact problems…….7

2c Test problem geometry and coordinates for Steuermann contact problems..……12

2d Test problem geometry and coordinates for flat punch contact problems…….15

3a Coarse mesh for FEA: patch tests with aligned nodes.....19

3a′ Coarse mesh for FEA: patch tests with misaligned nodes.....19

3b Coarse mesh for FEA: Hertzian contact…….20

3c Coarse mesh for FEA: Steuermann contact.....20

3d Coarse mesh for FEA: flat punch contact.....21

4a Convergence of contact stress distribution: Hertzian contact of a cylinder……....25

4b Convergence of contact stress distribution: Steuermann contact with $r_e / b = 1/3$.....25

ABSTRACT

The ANSYS code offers stress analysts a variety of contact element options: point-to-surface or surface-to-surface and low-order or high-order elements, in concert with any one of five contact algorithms (augmented Lagrangian, penalty method, etc.). This raises questions as to what option performs best under what circumstances. Here we offer some answers to these questions by examining performance in some numerical experiments.

The numerical experiments focus on frictionless contact with a rigid indenter; even so, the number of experiments involved is quite large. The experiments use a battery of test problems with known analytical solutions: contact patch tests with nodes matching and nonmatching, Hertzian contact of a cylinder and a sphere, and Steuermann contact of a strip punch with three different edge radii. For each of these test problems, three successively systematically-refined meshes are used to examine convergence. All told, over five hundred finite element analyses are run.

Results for this class of problems are the same for the augmented Lagrangian (AL, the default) and the penalty method (PM) algorithms. There is also no difference between results found with the two Lagrange multiplier (LM) algorithms. Thus together with results for the fifth contact algorithm (IMC-internal multipoint constraint), we have but three distinct sets of results.

The results for the AL and PM algorithms are good for all problems provided they are used with surface-to-surface elements. The results for the LM algorithms can be quite sensitive to matching of the nodes on the indented material with those on the indenter. When nodes matched, these algorithms also gave good results. The IMC algorithm, while

the fastest, did not give good results for the problems examined. When algorithms worked well, there was little difference in accuracy between low-order and high-order elements.

1 INTRODUCTION

1.1 Background and Motivation

Contact problems occur frequently in engineering stress analysis: Johnson (Reference 1) provides a useful overview of known solutions. Unfortunately, most of the configurations encountered in practice are too complex to be amenable to solution via the classical methods of References 1, 2. An example is the dovetail attachment used in a jet engine to attach blades to disks (see Figure 1). Herein σ_o represents the pull exerted by the remainder of the blade due to rotation. This pull is restrained by contact (e.g., on *C′*-*C*) and this in turn results in high contact stresses which play critical roles in the fatigue of such attachments. To resolve these key stresses, finite element analysis (FEA) is a natural tool, and indeed ANSYS contact elements have been used successfully to analyze the configuration in Figure 1 (see Reference 3).

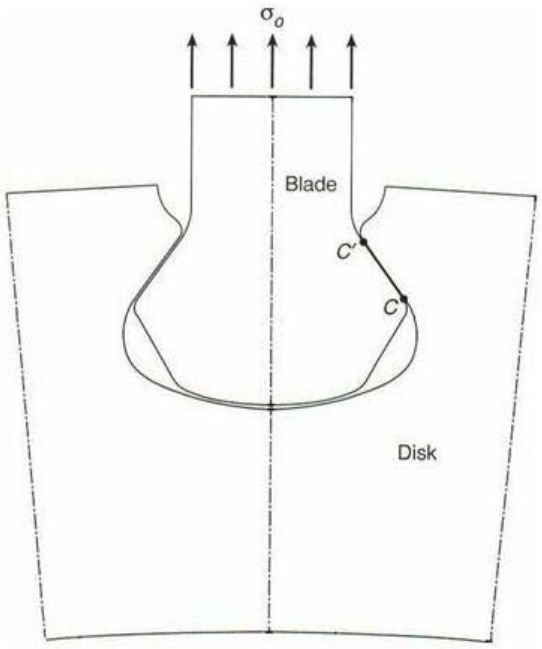

Figure 1: Dovetail blade attachment for a gas turbine engine

For such FEA, ANSYS provides the stress analyst with a number of options: point-to-surface or surface-to-surface and low-order or high-order elements in concert with any one of five contact algorithms –augmented Lagrangian (AL), penalty method (PM), Lagrange multiplier on contact normal and penalty on tangent (LMP), pure Lagrange multiplier on contact normal and tangent (PLM),and internal multipoint constraint (IMC). While ANSYS documentation (Reference 4) of these options provides some helpful guidance for their use, it stops short of telling the analyst which option is best under what circumstances. Here, then, we seek to provide some guidance in this respect.

1.2 Basic Approach

The basic means of providing this guidance is via an examination of the performance of these various contact options on an array of true contact test problems. That is, contact problems with known analytical solutions. These known solutions enable an unambiguous assessment of the errors attending the implementation of each of the contact options.

Here the test problems all involve indentation of an elastic half-space. Some care is needed, therefore, to ensure that appropriate boundary conditions are met on a finite region within this elastic half-space so that we still have true test problems.

In addition, here all the test problems only entail frictionless rigid indenters. However, within this restricted class of contact problems, quite a variety of configurations is examined, the hope being that the resulting numerical experiments will approach being comprehensive for this class.

1.3 Outline of Remainder of Paper

In what follows, we first describe the battery of test problems used. Next we provide details of their FEA using all of the preceding options. Thereafter we discuss the relative performance of these options as indicated by the results they produce on all the test problems (detailed stress results are appendicized). We close with some remarks in the light of this assessment.

2 TEST PROBLEMS

Here we provide formal statements and solutions for the following test problems: contact patch tests (both plane strain and axisymmetric cases), Hertzian contact of a cylinder and a sphere, Steuermann contact of three different strip punches with rounded edges, and contact of flat-ended punches (both plane strain and axisymmetric cases). This last is included, even though it is a singular problem, to complete the sequence of problems as edge radii go to zero; it also provides a test of whether or not contact algorithms diverge as they should for a singular problem.

2.1 Contact Patch Test (Problem *P*)

The specifics of the geometry for the plane strain patch test, Problem P_p , are as follows. We have a rigid strip, of width 2*a,* pressed into an elastic slab, also of width 2*a,* by a pressure p (Figure 2 (a)). The two are assumed to be perfectly aligned so that 2*a* is the extent of contact region. The geometry is readily framed in rectangular Cartesian coordinates (*x, z*) (see Figure 2 (a)). We use symmetry to restrict attention to one half of the slab which is denoted by R_p . Thus

$$R_p = \{(x, z) \mid 0 < x < a,\ 0 < z < h\} \tag{1}$$

where *h* is the height of the slab. With these geometric preliminaries in place we can formally state Problem P_p as follows.

In general, we seek the stresses $\sigma_x, \sigma_z, \tau_{xz}$, and their associated displacements *u, w,* as functions of *x* and *z* throughout R_p, satisfying: the field equations of elasticity which here consist of the stress equations of equilibrium in the absence of body forces and the stress-

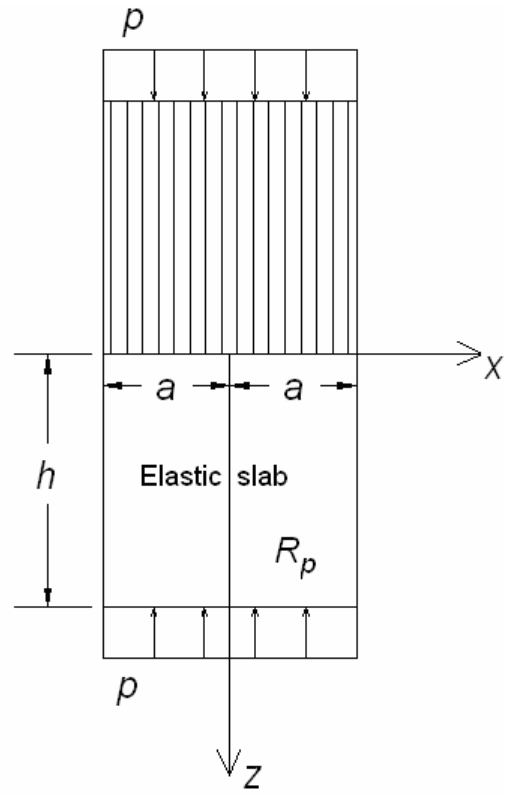

Figure 2a: Test problem geometry and coordinates for contact patch tests

displacement relations for a homogeneous and isotropic, linear elastic solid in a state of plane strain; the symmetry conditions,

$$u = 0 \qquad \tau_{xz} = 0 \tag{2}$$

on $x = 0$ for $0 < z < h$; the applied pressure conditions,

$$\sigma_z = -p \qquad \tau_{xz} = 0 \tag{3}$$

on $z = h$ for $0 < x < a$; the stress-free conditions,

$$\sigma_x = 0 \qquad \tau_{xz} = 0 \tag{4}$$

on $x = a$ for $0 < z < h$; and the frictionless contact conditions,

$$w = 0 \qquad \tau_{xz} = 0 \tag{5}$$

In particular, for this test problem we are interested in the stress response for which there is the following elementary analytical solution

$$\sigma_z = -p \qquad \sigma_x = \tau_{xz} = 0 \tag{6}$$

throughout R_p.

The axisymmetric counterpart, Problem P_a, replaces the rigid strip and elastic slab with rigid and elastic cylinders. It can be framed in cylindrical coordinates (*r, z*) where, in effect, *r* takes over the role of *x*. Thus the region of interest becomes

$$R'_p = \{(r, z) \mid 0 < r < a,\ 0 < z < h\} \tag{7}$$

The formulation is then analogous, as is the solution which has

$$\sigma_z = -p \qquad \sigma_r = \tau_{rz} = 0 \tag{8}$$

2.2 Hertzian Contact (Problem *H*)

The specifics of the geometry for the plane strain Hertzian contact problem, Problem H_p, are as follows. We have a rigid cylinder of radius *R* pressed into an elastic half-space by a force per unit length of P (shown schematically in Figure 2 (b)). For FEA, the half-space is represented by a rectangular block of width 8*a* and length 4*a,* where 2*a* is the extent of contact region (*a*<<*R*).The geometry is framed in rectangular Cartesian coordinates (*x, z*) (see Figure 2 (b)). We use symmetry to restrict attention to one half of the slab which is denoted by R_h. Thus

$$R_h = \{(x, z) \mid 0 < x < 4a,\ 0 < z < 4a\} \tag{9}$$

With these geometric preliminaries in place we can formally state Problem H_p as follows.

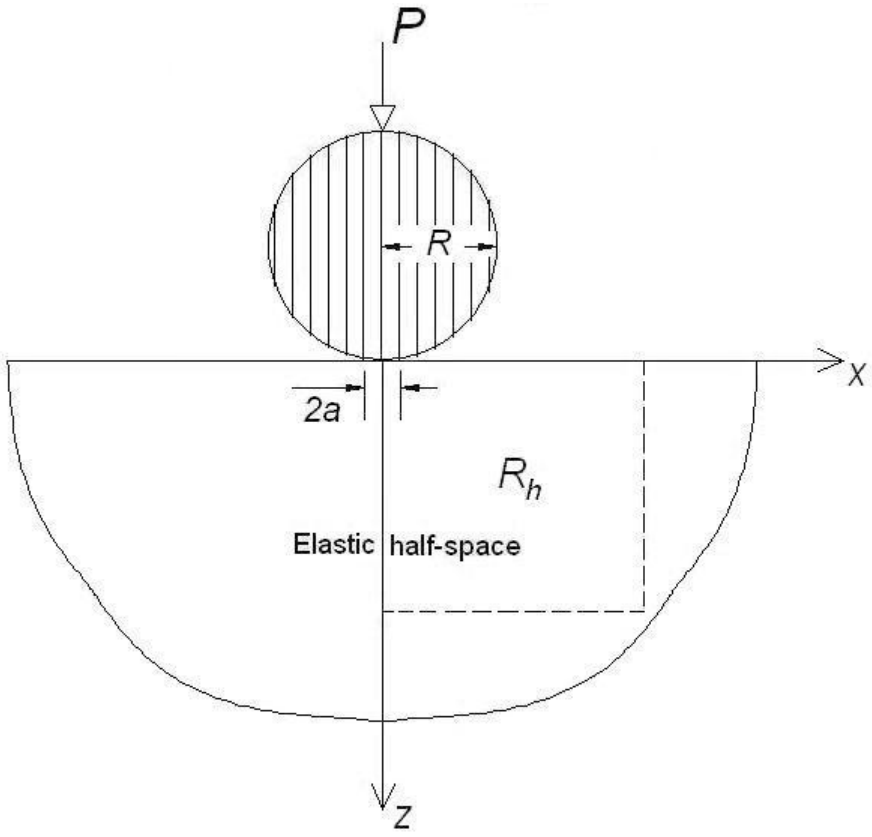

Figure 2b: Test problem geometry and coordinates for Hertzian contact problems

In general, we seek the plane strain stresses $\sigma_x, \sigma_z, \tau_{xz}$, and their associated displacements *u, w,* as functions of *x* and *z* throughout R_h, satisfying: the field equations of elasticity; the symmetry conditions,

$$u = 0 \qquad\qquad \tau_{xz} = 0 \tag{10}$$

on $x = 0$ for $0 < z < 4a$; the far-field applied traction conditions,

$$\sigma_z = -\frac{4p}{\pi a} m\left(1 - \frac{z^2 + n^2}{m^2 + n^2}\right)$$

$$\tau_{xz} = \tau_{xz}^{M} = -\frac{4p}{\pi a} n\left(\frac{m^2 - z^2}{m^2 + n^2}\right) \tag{11}$$

on $z = 4a$ for $0 < x < 4a$, and

$$\sigma_x = -\frac{4p}{\pi a}\left\{m\left(1 + \frac{z^2 + n^2}{m^2 + n^2}\right) - 2z\right\}$$

$$\tau_{xz} = \tau_{xz}^{M} \tag{12}$$

on $x = 4a$ for $0 < z < 4a$, where

$$m^2 = \frac{1}{2}\left[\left(\left(a^2 - x^2 + z^2\right)^2 + 4x^2z^2\right)^{1/2} + \left(a^2 - x^2 + z^2\right)\right]$$

$$n^2 = \frac{1}{2}\left[\left(\left(a^2 - x^2 + z^2\right)^2 + 4x^2z^2\right)^{1/2} - \left(a^2 - x^2 + z^2\right)\right]$$

and $p = P/2a$ is the applied pressure in the contact region; the stress-free conditions, outside of contact,

$$\sigma_z = 0 \qquad\qquad \tau_{xz} = 0 \tag{13}$$

on $z = 0$ for $a < x < 4a$; and the frictionless contact conditions,

$$w = \frac{a^2 - x^2}{2R} \qquad\qquad \tau_{xz} = 0 \tag{14}$$

on $0 \le x \le a$. In particular, we are interested in the contact stresses for which there are the following exact solutions from Hertz (Reference 5- see page 101 of Reference 1):

$$\sigma_z = \sigma_x = -\frac{4p}{\pi}\sqrt{1 - \left(\frac{x}{a}\right)^2} \tag{15}$$

on $z = 0$.

Some comments on the preceding formulation are in order. The far-field stresses here in Equations (11), (12) are taken from McEwen (Reference 6- see pages 102-104 of Reference 1), and are the exact interior stresses for plane strain Hertzian contact of a cylinder on a half-space. Thus they furnish the exact tractions on the boundary of R_h. The contact extent a is taken as given here. In fact, it has to be determined in the analysis of the problem as p is applied. From Hertz (Reference 5- see page 427 of Reference 1), these two are related by

$$a = \frac{8R\left(1-\nu^2\right)}{\pi E} p \tag{16}$$

where E is Young's modulus and ν is Poisson's ratio of the half-space.

The axisymmetric counterpart, Problem H_a, replaces the rigid cylinder and elastic rectangular block with rigid sphere and elastic cylinder. It can be framed in cylindrical coordinates (r, z) where, in effect, r takes over the role of x. The region of interest now becomes

$$R_h' = \{(r, z) \mid 0 < r < 8a,\ 0 < z < 8a\} \tag{17}$$

With these geometric preliminaries in place we can formally state Problem H_a as follows.

In general, we seek the axisymmetric stresses $\sigma_r, \sigma_z, \tau_{rz}$, and their associated displacements u_r, w, as functions of r and z throughout R_h', satisfying: the field equations of elasticity; the far-field applied traction conditions,

$$\sigma_z = \sigma_z^B = -\frac{3a^2}{2}\frac{z^3}{\rho^5} p$$

$$\tau_{rz} = \tau_{rz}^B = -\frac{3a^2}{2}\frac{rz^2}{\rho^5} p \tag{18}$$

on $z = 8a$ for $0 < r < 8a$, and

$$\sigma_r = \sigma_r^B = \frac{pa^2}{2}\left(\frac{(1-2\nu)}{r^2}\left(1-\frac{z}{\rho}\right)-\frac{3r^2 z}{\rho^5}\right)$$

$$\tau_{rz} = \tau_{rz}^B \tag{19}$$

on $r = 8a$ and $0 < z < 8a$, where $\rho = (r^2 + z^2)^{1/2}$ and p now equals $P/\pi a^2$; the stress-free conditions, outside of contact,

$$\sigma_z = 0 \qquad\qquad \tau_{rz} = 0 \tag{20}$$

on $z = 0$ for $a < r < 8a$; and the frictionless contact conditions,

$$w = \frac{a^2 - r^2}{2R} \qquad\qquad \tau_{rz} = 0 \tag{21}$$

on $0 \le r \le a$. In particular, we are interested in the contact stress for which there is the following exact solution from Hertz (Reference 5- see pages 92, 93 of Reference 1):

$$\sigma_z = -\frac{3p}{2}\sqrt{1-\left(\frac{r}{a}\right)^2} \tag{22}$$

on $z = 0$.

Some comments on the preceding formulation are in order. The far-field stresses here in Equations (18), (19) are taken from Boussinesq's point load (Reference 1, page 51). Thus they are only approximate to the true boundary conditions, but they are asymptotic to them in a St. Venant sense. To check that such asymptotic behavior is adequate, we actually solve the problem by successively doubling the extent of R_h' until no changes occur in the contact solution of Equation (22). This is how we in fact arrive at $8a$. Too, as earlier, the contact extent a is taken as given here. In fact, it has to be determined in the

analysis of the problem as p is applied. From Hertz (Reference 5- see page 427 of Reference 1), these two are related by

$$a = \frac{3\pi R\left(1-\nu^2\right)}{4E} p \tag{23}$$

2.3 Steuermann Contact (Problem *S*)

The specifics of the geometry for the plane strain Steuermann contact problem, Problem S_p, are as follows. A rigid flat punch with rounded edges that has a flat section of width 2*b,* and edge radii r_e, is pressed into an elastic half-space by a force per unit length of P (Figure 2 (c)). The punch makes contact with the half-space over a strip of width 2*a* (*a* > *b*). For FEA, the half-space is represented by a rectangular block of width 16*b* and length 8*b*. The geometry is readily framed in rectangular Cartesian coordinates (*x*, *z*) (see Figure 2 (c)). We use symmetry to restrict attention to one half of the block which is denoted by R_s. Thus

$$R_s = \{(x, z) \mid 0 < x < 8b,\ 0 < z < 8b\} \tag{24}$$

With these geometric preliminaries in place we can formally state Problem S_p as follows.

In general, we seek the plane strain stresses $\sigma_x, \sigma_z, \tau_{xz}$, and their associated displacements *u, w*, as functions of *x* and *z* throughout R_s, satisfying: the field equations of elasticity; the symmetry conditions,

$$u = 0 \qquad\qquad \tau_{xz} = 0 \tag{25}$$

on $x = 0$ for $0 < z < 8b$; the far-field roller restraint conditions,

$$w = 0 \qquad\qquad \tau_{xz} = 0 \tag{26}$$

on $z = 8b$ for $0 < x < 8b$; the far-field stress-free conditions,

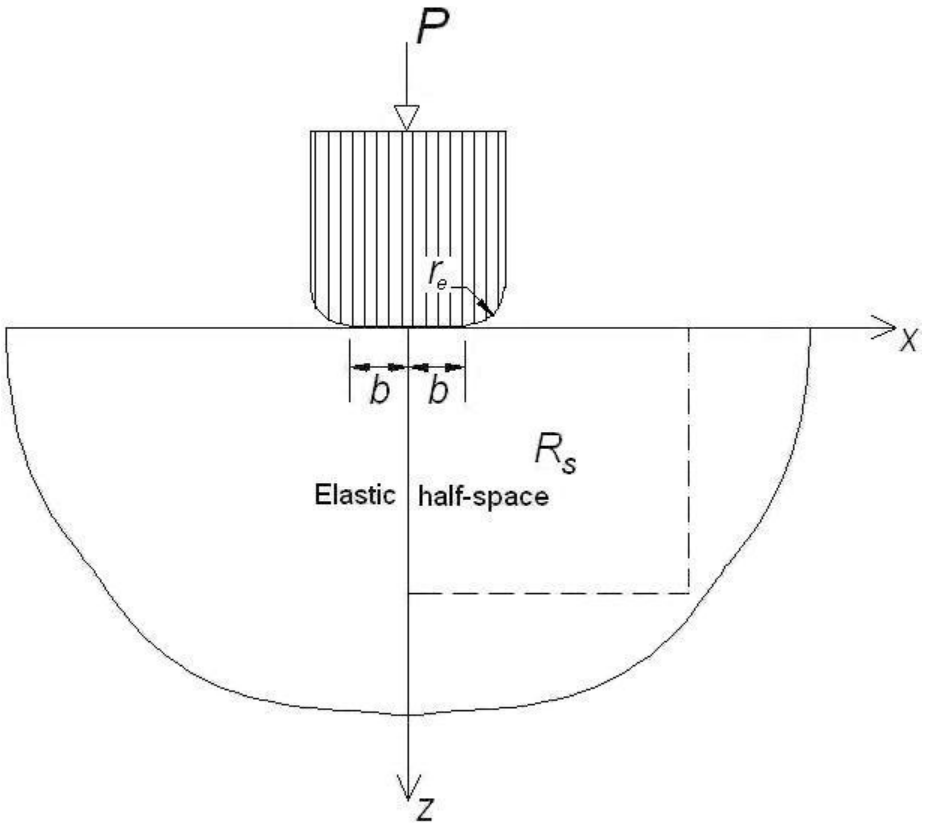

Figure 2c: Test problem geometry and coordinates for Steuermann contact problems

$$\sigma_x = 0 \qquad \tau_{xz} = 0 \tag{27}$$

on $x = 8b$ for $0 < z < 8b$; the stress-free conditions, outside of contact,

$$\sigma_z = 0 \qquad \tau_{xz} = 0 \tag{28}$$

on $z = 0$ for $a < x < 8b$; and the frictionless contact conditions,

$$w = \delta \qquad \tau_{xz} = 0 \tag{29}$$

on $z = 0$ for $0 \le x \le b$,where δ is the depth of penetration, and

$$w = \delta - \frac{(x-b)^2}{2r_e} \qquad \tau_{xz} = 0 \tag{30}$$

on $z = 0$ for $b \le x \le a$. In particular, we are interested in the contact stress for which there is the following analytical solution from Steuermann (Reference 7 as reported in Reference 8):

$$\frac{a}{P}\sigma_z = -\frac{2/\pi}{\pi - 2\phi_0 - \sin 2\phi_0} \times \left((\pi - 2\phi_0)\cos\phi + \ln\left[\left| \frac{\sin(\phi + \phi_0)}{\sin(\phi - \phi_0)} \right|^{\sin\phi} \times \left| \tan\frac{\phi + \phi_0}{2} \tan\frac{\phi - \phi_0}{2} \right|^{\sin\phi_0} \right] \right) \tag{31}$$

on $z = 0$ for $0 < x < a$, where $a = b/\sin\phi_0$, $\sin\phi = (x/b)\sin\phi_0$, and the angle ϕ_0 implicitly specifies the contact width, *a*, and may be obtained as a function of the load *P* from

$$\frac{2r_e(1-\nu^2)}{b^2 E} P = \frac{\pi - 2\phi_0}{2\sin^2\phi_0} - \cot\phi_0 \tag{32}$$

Some comments on the preceding problem statement in order. Here we use rollers on boundary instead of applied tractions because it is observed in Hertzian contact that using only rollers on the boundary at a depth of about 8*a* leaves σ_z at $z = 0$ unchanged. Thus they are safely used here since we are particularly interested in the contact stress, σ_z. Again as previously, the contact extent *a* is taken as given here. In fact, it has to be determined in the analysis of the problem as P is applied. These two are related as in Equation (32).

Some further specifications are required for the FEA of this class of problem. First r_e / b needs to be set: Here we take this to be 1, 1/3, and 1/7 to produce a range of stress concentrations similar to those encountered in practice (e.g., Reference 3). Second Poisson's ratio ν needs to be prescribed: Here we simply take this to be the representative value of 1/4. Third and last, the relative pressure has to be set: Here we

take $p/E = 1/1000$, again a choice which leads to stress concentrations similar to those encountered in practice.

2.4 Flat Punch Contact (Problem *F*)

The specifics of the geometry for the plane strain, flat punch, contact problem, Problem F_p, are as follows. A rigid flat strip punch of width 2*a* is pressed into an elastic half-space by a pressure p (Figure 2 (d)). Because the punch has sharp corners, it makes contact with the half-space over its entire width 2*a.* For FEA, the half-space is represented by a rectangular block of width 8*a* and length 4*a*. The geometry is readily framed in rectangular Cartesian coordinates (*x, z*) (see Figure 2 (d)). We use symmetry to restrict attention to one half of the block which is denoted by R_f .Thus

$$R_f = \{(x, z) \mid 0 < x < 4a,\ 0 < z < 4a\} \tag{33}$$

With these geometric preliminaries in place we can formally state Problem F_p as follows. In general, we seek the plane strain stresses $\sigma_x, \sigma_z, \tau_{xz}$, and their associated displacements *u, w*, as functions of *x* and *z* throughout R_f, satisfying: the field equations of elasticity; the symmetry conditions,

$$u = 0 \qquad\qquad \tau_{xz} = 0 \tag{34}$$

on $x = 0$ for $0 < z < 4a$; the far-field applied traction conditions,

$$\sigma_z = -\frac{p}{2\pi}\{2(\theta_1 - \theta_2) - (\sin 2\theta_1 - \sin 2\theta_2)\}$$

$$\tau_{xz} = \tau_{xz}^S = \frac{p}{2\pi}(\cos 2\theta_1 - \cos 2\theta_2) \tag{35}$$

on $z = 4a$ for $0 < x < 4a$, and

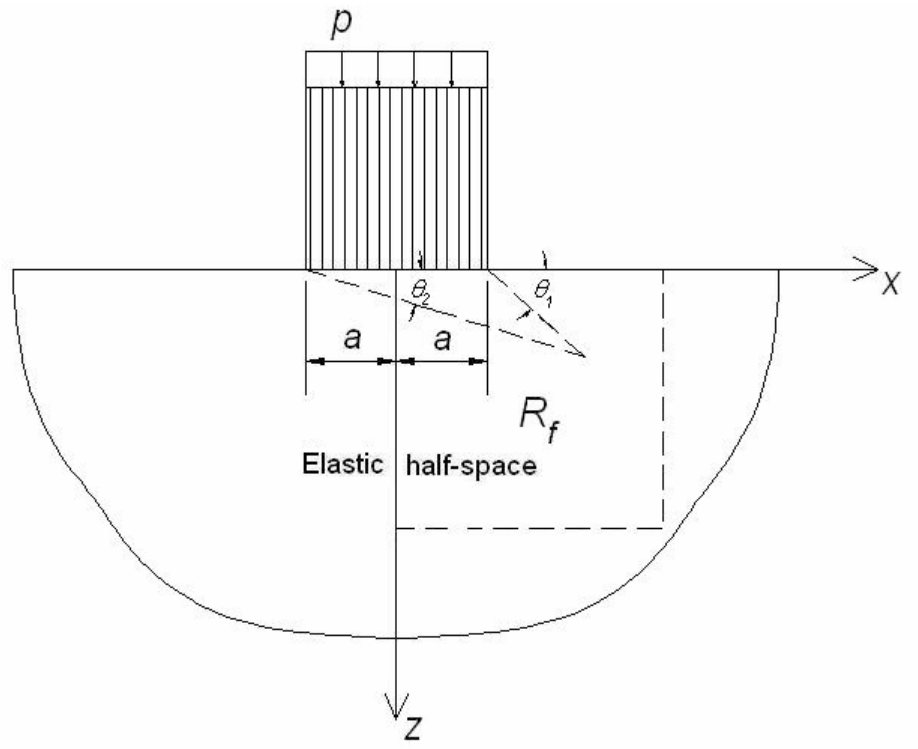

Figure 2d: Test problem geometry and coordinates for flat punch contact problems

$$\sigma_x = -\frac{p}{2\pi}\{2(\theta_1 - \theta_2) + (\sin 2\theta_1 - \sin 2\theta_2)\}$$

$$\tau_{xz} = \tau_{xz}^S \tag{36}$$

on $x = 4a$ for $0 < z < 4a$, where $\tan\theta_i = z/(x + (-)^i a), i = 1, 2$ (see Figure 2 (d)); the stress-free conditions, outside of contact,

$$\sigma_z = 0 \qquad\qquad \tau_{xz} = 0 \tag{37}$$

on $z = 0$ for $a < x < 4a$; and the frictionless contact conditions,

$$w = \delta \qquad\qquad \tau_{xz} = 0 \tag{38}$$

on $z = 0$ for $0 \le x \le a$, where δ is the depth of penetration. In particular, we are interested in the contact stress for which there is the following analytical solution from Sadowsky (Reference 9- see page 37 of Reference 1):

$$\sigma_z = -\frac{2pa}{\pi\sqrt{a^2 - x^2}} \tag{39}$$

on $z = 0$.

Some comments on the preceding formulation are in order. The far-field stresses here in Equations (35), (36) are for a uniform strip load on a half-space (see Reference 1, page 21). Thus they are only approximate to the true boundary conditions, but they are asymptotic to them in a St. Venant sense. To check that such asymptotic behavior is adequate, we actually solve the problem by successively doubling the extent of the block approximating the half-space until no changes occur in the contact solution: We find this to be the case for R_f of Equation (33).

The axisymmetric counterpart, Problem F_a, replaces the flat strip punch and elastic block with cylinders. It can be framed in cylindrical coordinates (*r, z*) where, in effect, *r* takes over the role of *x*. Thus the region of interest becomes

$$R'_f = \{(r, z) \mid 0 < r < 4a,\ 0 < z < 4a\} \tag{40}$$

With these geometrical preliminaries in place we can formally state Problem F_a as follows.

In general, we seek the axisymmetric stresses $\sigma_r, \sigma_z, \tau_{rz}$, and their associated displacements u_r, w, as functions of *r* and *z* throughout R'_f, satisfying: the field equations of elasticity; the far-field applied traction conditions,

$$\sigma_z = \sigma_z^B \qquad\qquad \tau_{rz} = \tau_{rz}^B \tag{41}$$

on $z = 4a$ for $0 < r < 4a$, and

$$\sigma_r = \sigma_r^B \qquad\qquad \tau_{rz} = \tau_{rz}^B \tag{42}$$

on $r = 4a$ for $0 < z < 4a$; the stress-free conditions, outside of contact,

$$\sigma_z = 0 \qquad\qquad \tau_{rz} = 0 \tag{43}$$

on $z = 0$ for $a < r < 4a$; the frictionless contact conditions,

$$w = \delta \qquad\qquad \tau_{rz} = 0 \tag{44}$$

on $z = 0$ for $0 \le r \le a$. In particular, we are interested in the contact stress for which there is the following analytical solution from Harding and Sneddon (Reference 10- see pages 59, 60 of Reference 1):

$$\sigma_z = -\frac{a}{2\sqrt{a^2 - r^2}}\, p \tag{45}$$

on $z = 0$.

Some comments on the preceding formulation are in order. The far-field stresses here in Equations (41), (42) are taken from Boussinesq's point load (Equations (18), (19)). Thus they are only approximate to the true boundary conditions, but they are asymptotic to them in a St. Venant sense. To check that such asymptotic behavior is adequate, we actually solve the problem by successively doubling the extents of the cylinder approximating the half-space: We find this to be the case for R'_f of Equation (40).

3 FINITE ELEMENT ANALYSIS

For the FEA of the previous problems, we not only discretize the indented material, but also the indenter. We then take of $E_e / E_r = 1/10^6$, where E_e is Young's modulus for the elastic indented material, E_r is that for the relatively rigid indenter. We find no difference in results when $E_e / E_r = 1/10^7$, so judge the first ratio to be sufficient to replicate indentation by a rigid indenter.

For this discretization we use four-node quadrilateral (4Q) and eight-node quadrilateral (8Q) elements (ANSYS elements PLANE42 and PLANE82 for plane strain problems, the same elements with the axisymmetric option for axisymmetric problems, Reference 4). For the most part, we use a largely uniform element distribution (see Figure 3, parts (a) (b) and (d)). The exception is for the Steuermann problem where we employ some element refinement near the edge of contact to capture the high stress gradients there more effectively (see Figure 3 (c)). We also align nodes, or nearly align nodes, on the surface of the indenter with those on the surface of the indented material. This is understood to be the arrangement that most facilitates running contact elements. We do this throughout except for the contact patch test: Herein, Problem *P* (both plane strain and axisymmetric versions) has nodes aligned, while Problem P' (both plane strain and axisymmetric versions) does not (see Figure 3 (a′)). We deliberately misalign nodes here to investigate effects on the contact algorithms because in the complex configurations encountered in practice it is not always possible to align nodes.

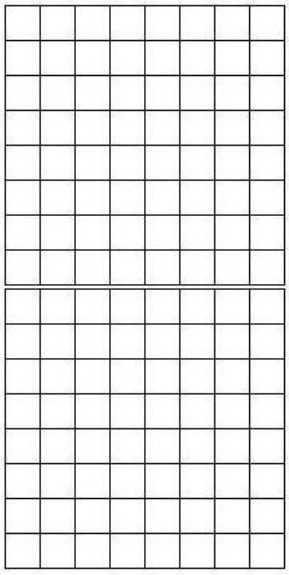

Figure 3a: Coarse mesh for FEA- patch tests with aligned nodes

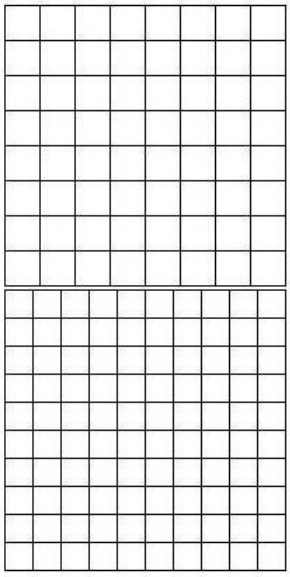

Figure 3a′: Coarse mesh for FEA- patch tests with misaligned nodes

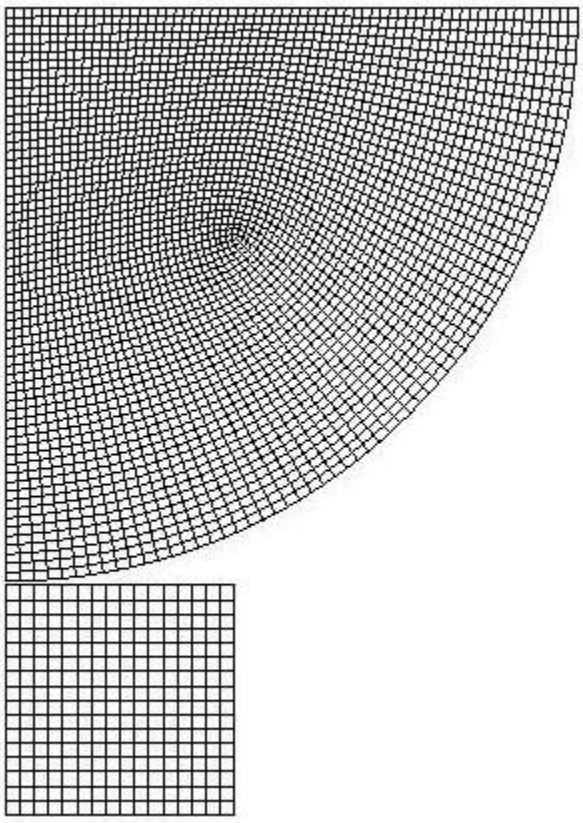

Figure 3b: Coarse mesh for FEA- Hertzian contact

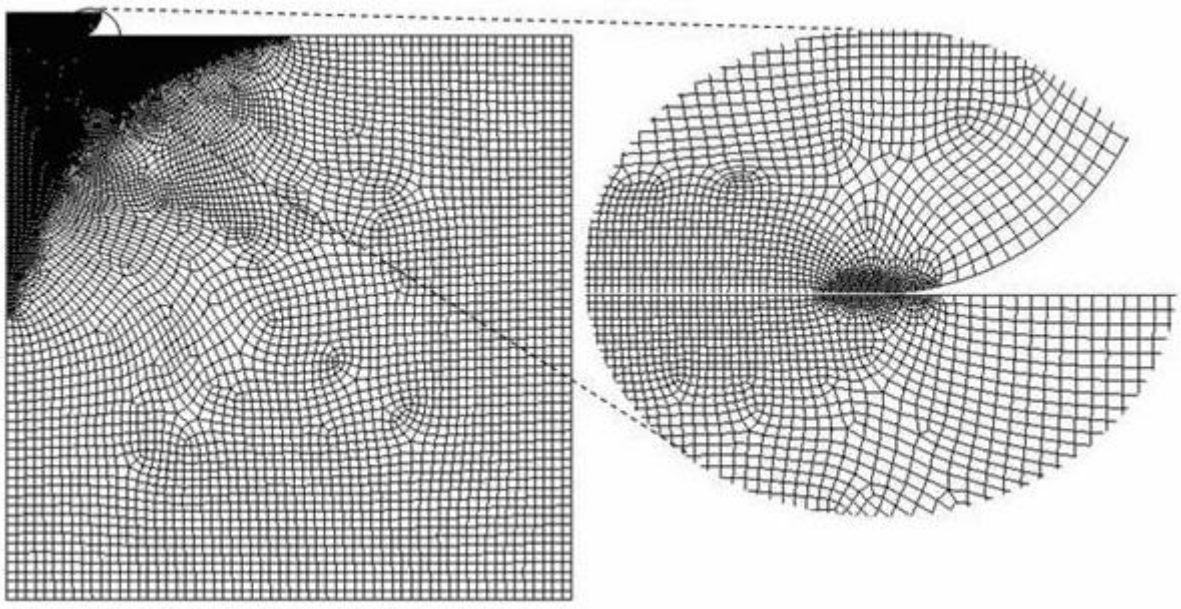

Figure 3c: Coarse mesh for FEA- Steuermann contact

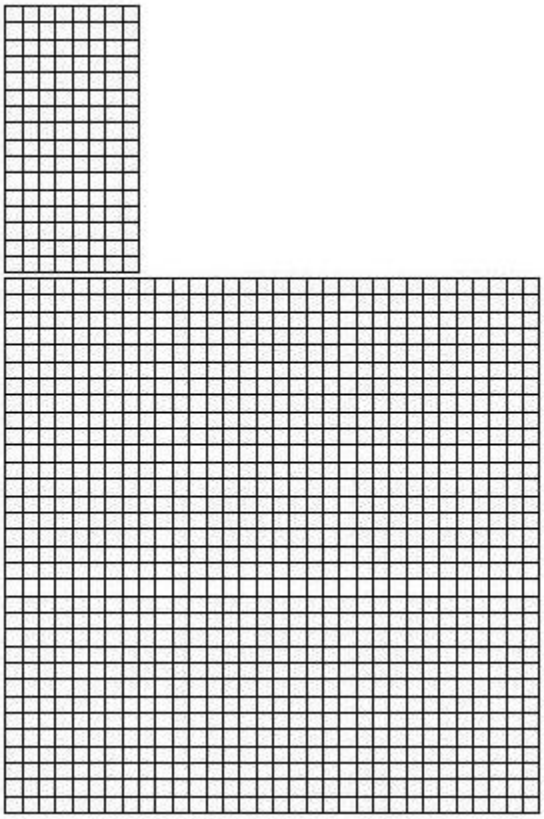

Figure 3d: Coarse mesh for FEA- flat punch contact

To police the contact conditions between the geometries, we use surface-to-surface (CONTA172 and TARGE169, Reference 4) or node-to-surface (CONTA175 and TARGE169, Reference 4) contact elements. These contact elements overlie the spatial elements on contact surfaces at $z = 0$. An important element-type option for these contact elements (CONTA172 and CONTA175) is the contact algorithm (KEYOPT 2) with which they are used in ANSYS. A selection for this algorithm can be made from the following five different contact algorithms: Augmented Lagrangian (AL, default, KEYOPT (2)=0), penalty method (PM, KEYOPT (2)=1), Lagrange multiplier on contact normal and penalty on tangent (LMP, KEYOPT (2)=3), pure Lagrange multiplier on

contact normal and tangent (PLM, KEYOPT (2)=4), and internal multipoint constraint (IMC, KEYOPT (2)=2). We employ all of these options in our analysis.

As described in ANSYS documentation (Reference 4), the AL method is an iterative series of penalty methods, which use a contact 'spring' to establish a relationship between the two contact surfaces where the spring stiffness is called the contact stiffness. Compared to the PM, AL method is expected to lead to better conditioning and is less sensitive to the magnitude of the contact stiffness. The LMP and PLM algorithms enforce zero penetration when contact is closed. While the LMP algorithm allows a small amount of slip for the sticking contact condition, the PLM algorithm enforces 'zero slip'. Both do not require contact stiffness. The IMC algorithm is used in conjunction with bonded contact and no separation contact to model several types of contact assemblies and kinematic constraints.

When employing these options, the auto CNOF/ICONT adjustment in element type options for contact elements is set to 'close gap' (KEYOPT (5)=1). Further, we use automatic time stepping with a small time step size(<1) to enhance convergence for some algorithms which perform weakly with default settings (LMP, PLM in Problem *H*).

To examine convergence, we fairly systematically refine each mesh twice by successively halving element sides. This generates coarse meshes (C, h), medium meshes (M, $h/2$), and fine meshes (F, $h/4$), where h is linear measure of representative element size. The coarse meshes are the ones shown in Figure 3. Element numbers for all three meshes for the elastic indented material and the various problems are set out in Table 1.

Table 1 : Element numbers in meshes for problems

Mesh	P	P'	H	S			F
				$r_e / b = 1$	$r_e / b = 1/3$	$r_e / b = 1/7$	
C	64	100	256	8372	16222	16809	1024
M	256	400	1024	33488	64888	67236	4096
F	1024	1600	4096	133952	259552	268944	16384

4 ASSESSMENT OF ELEMENT PERFORMANCE AND CONCLUSIONS

In Figure 4 we show some representative contact stresses. These are for the plane strain Hertzian contact and Steuermann contact when $r_e / b = 1/3$. Apparent for both configurations is that the convergence of peak stress values and the extents of contact present the greatest challenges to the contact elements. These aspects are the slowest in terms of converging, though they are converging with mesh refinement in Figure 4 (that is, moving closer to the exact solutions). Thus we focus on peak stress values henceforth. In making this choice, we are also tracking extents of contact to some degree because peak values cannot really converge until contact extents are accurately captured. The exceptions in this regard are the contact patch tests wherein the exact solutions are constant: For these, we focus on the biggest positive deviation or maximum normalized stress above unity (similar results are obtained if we use the minimum instead).

Accordingly, with a view to summarizing the plethora of FEA results, we now confine attention to just such single stress components at single locations. The precise stresses chosen to this end are defined in the Appendix. Even with this condensation, results are extensive (there are 43 tables in the Appendix).

To classify performance for the stresses in the Appendix, we grade *accuracy* as follows

$$\mathbf{e} < 1 \leq \mathbf{g} < 5 \leq \mathbf{s} < 10 \leq \mathbf{u} \tag{46}$$

where **e** is excellent, **g** is good, **s** is satisfactory, and **u** is unsatisfactory, and numbers are percentage errors. This grading system reflects the sort of accuracy typically sought in practice. Certainly other percentages could be adopted: It is not expected that other choices would change what follows significantly.

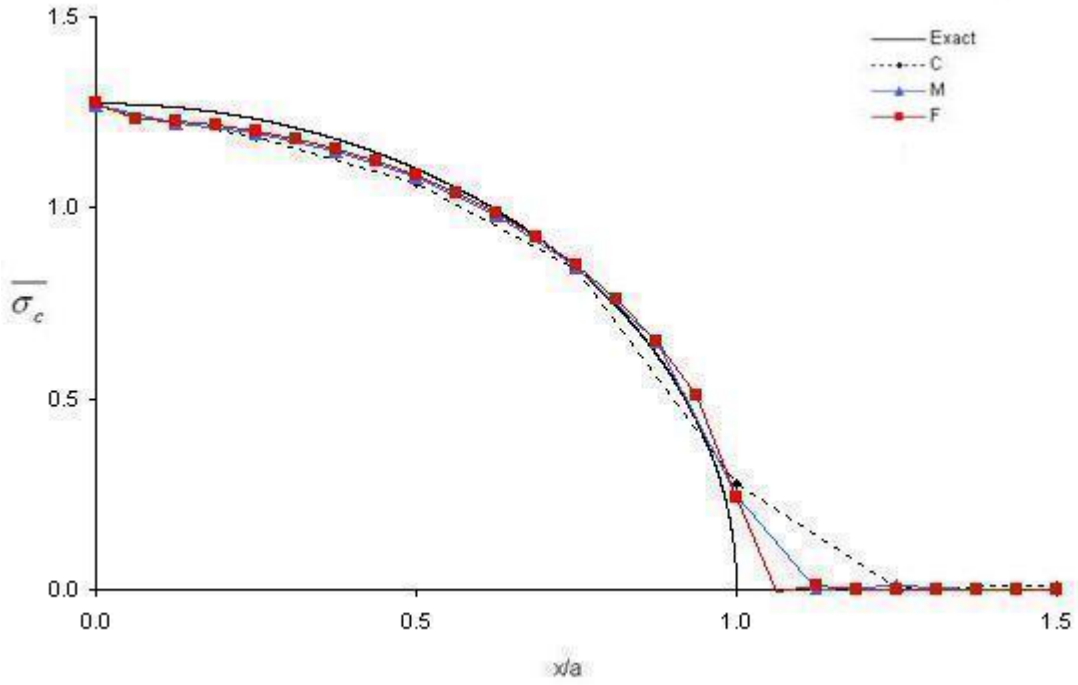

Figure 4a: Convergence of contact stress distribution: Hertzian contact of a cylinder

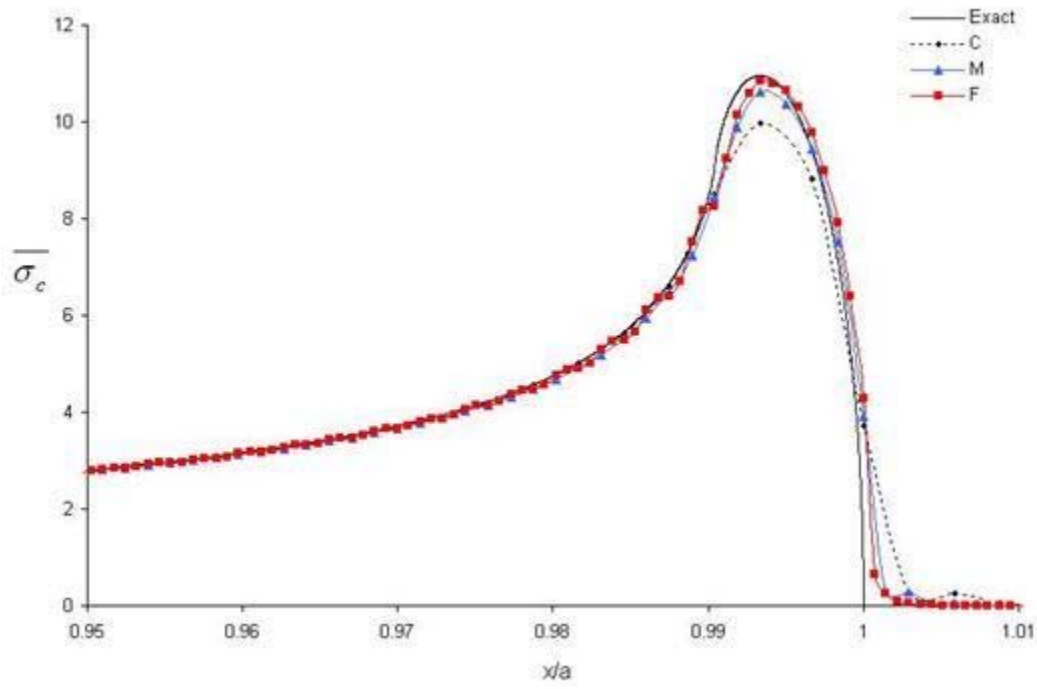

Figure 4b: Convergence of contact stress distribution- Steuermann contact with $r_e / b = 1/3$

We also classify performance as to whether or not it is *converging*. Convergence is indicated by the letter 'c'. Of course, this check is only applied to nonsingular problems, the flat punch problems where we expect and want divergence being excluded.

Performance for all nonsingular problems is thus summarized in Table 2. Herein there are two rows of entries for Problem H_p, one for the contact stress, the other for the companion horizontal stress (see Appendix for precise definitions).

In Table 2, we have grouped results for the AL and PM algorithms, and for the LMP and PLM algorithms. This is because they are the same for these pairs of algorithms with frictionless contact. We have also not distinguished between surface-to-surface (ss) and node-to-surface (ns) for LMP, PLM and IMC: Again, this is because results are essentially the same.

Several trends are apparent in Table 2. First, the default algorithm AL (and therefore also PM) performs at a good-excellent level with 4Q elements and the ss option except for the Steuermann problems with smaller radii. It performs nearly as well with 8Q elements. It performs almost uniformly less well with the ns option.

Second, the LMP, PLM option with 4Q elements performs pretty much at the good-excellent level except for when nodes are not aligned (Problem *P′*). If possible to align nodes in applications, this would appear to be the best option for the present class of problems. Performance drops off some for the LMP, PLM options with 8Q elements. This is not really surprising. Neither 4Q nor 8Q elements contain the square-root stress field present at the edge of contact. Thus there is no reason to expect better performance of higher-order elements in the vicinity of the edge of contact. What Table 2 shows is that, in fact, higher-order elements if anything perform less well than low-order.

Third, the performance of the IMC option is uniformly unsatisfactory on this set of experiments. It is possible that this performance could be improved with further mesh refinement.

Turning to *convergence*, this is somewhat erratic with contact problems. This is because there are two aspects that the FEA is seeking with mesh refinement: the magnitude of the peak stresses involved as well as the location of the edge of contact. Once the latter is found, typically FEA converges well. This is reflected by the c's in Table 2. It is probable that in instances not demarked by c's with satisfactory or better results, further mesh refinement would lead to converging results.

For the singular flat-punch problems, it is important that contact elements *diverge*. This is because, in the event a singularity was inadvertently introduced into a contact problem, the stress analyst would then be alerted that this had occurred. Thus the futility of stress versus strength comparisons in the presence of a singularity could be avoided.

To assess whether or not FEA stresses are diverging, we use the following simple criterion which is numerically consistent with stresses increasing without bound. For a singular, and therefore diverging, stress component σ we expect

$$\left|\sigma_c - \sigma_m\right| < \left|\sigma_m - \sigma_f\right| \tag{47}$$

where the subscripts denote the mesh used to compute it (c…coarse, m…medium, f…fine). We find Equation (47) to be complied with for all contact elements and options.

In closing, we remark that there are a quite a number of options within the options considered here and that can be selected by the stress analyst (e.g., FKN normal penalty stiffness in AL and PM, FTOLN penetration tolerance, PINB pinball region).

Table 2a : Accuracy and convergence of 4Q elements

Problem (r_e/b)	Algorithm (ss or ns)			
	AL, PM (ss)	AL, PM (ns)	LMP, PLM	IMC
P_p	**e**, c	**s**	**e**	**u**
P_a	**g**	**u**	**e**	**u**
P_p'	**g**	**u**	**u**	**u**
P_a'	**s**	**u**	**u**	**u**
H_p	**e**, c	**u**	**g**	**u**
	g, c	**u**	**s**	**u**
H_a	**g**, c	**g**, c	**e**, c	**u**
$S(1)$	**s**	**s**	**g**, c	**u**, c
$S(1/3)$	**u**, c	**u**	**g**, c	**u**, c
$S(1/7)$	**u**, c	**u**	**g**, c	**u**, c

Table 2b : Accuracy and convergence of 8Q elements

Problem (r_e/b)	Algorithm (ss or ns)			
	AL, PM (ss)	AL, PM (ns)	LMP, PLM	IMC
P_p	**e**, c	**u**	**u**, c	**u**
P_a	**g**	**u**	**u**	**u**
P_p'	**s**	**u**	**u**, c	**u**
P_a'	**s**	**u**	**u**	**u**
H_p	**e**, c	**s**	**g**, c	**u**
	g, c	**u**	**s**, c	**u**
H_a	**g**	**s**	**s**, c	**u**, c
$S(1)$	**s**	**g**	**e**, c	**u**, c
$S(1/3)$	**u**	**e**, c	**e**, c	**u**, c
$S(1/7)$	**u**	**s**	**g**	**u**, c

We have used exclusively default values for these other options, and consequently can offer no commentary on the possible improvements these other options might offer. However, even without using these other options, performance of the AL, PM algorithms with surface-to-surface elements is good for most problems, and performance of the LMP, PLM algorithms is fine for any problems in which nodes can be aligned.

5 FUTURE WORK

Extension of the Steuermann contact problems to include the axisymmetric case (M. Ciavarella, Reference 11) would complete this set of problems considered here. This study would also be enhanced by the inclusion of elastic indenters wherever corresponding solutions exist (Problem *P*, *H*): Preliminary analysis completed to date indicates that contact algorithms are mostly seriously challenged by relatively rigid indenters rather than elastic indenters. It would also be good to consider the performance of other standard codes (e.g., ABAQUS). Ultimately, a study that included friction effects would provide users of these algorithms more complete guidance on their implementation, though such a study could be expected to be more difficult to undertake than the present one because of the shortage of exact solutions when friction acts.

REFERENCES

1) K.L. Johnson, *Contact Mechanics*. Cambridge University Press, 1985, Cambridge, England.

2) G.M.L. Gladwell, *Contact Problems in the Classical Theory of Elasticity*. Sijthoff and Noordhoff, 1980.

3) G.B. Sinclair, N.G. Cormier, J.H. Griffin, G. Meda, Contact stresses in dovetail attachments: finite element modeling. *Journal of Engineering for Gas Turbines and Power*, 2002, Vol. 124, pp. 182-189.

4) ANSYS personnel, *ANSYS Advanced Analysis Techniques*, Revision 9.0. ANSYS Inc., 2004, Canonsburg, Pennsylvania.

5) H. Hertz, On the contact of elastic solids. *Journal für die reine und angewandte Mathematik*, 1882, Vol. 92, pp. 156-171.

6) E. McEwen, Stresses in elastic cylinders in contact along a generatrix. *Philosophical Magazine*, 1949, Vol. 40, pp. 454-459.

7) I. Y. Steuermann, *Contact problem of the theory of elasticity*. Gostekhteoretizdat, 1949, Moscow-Leningrad. Available from the British library in an English translation by the Foreign Technology Division, 1970, FTD-MT-24-61-70.

8) M. Ciavarella, D.A. Hills, G. Monno, The influence of rounded edges on indentation by a flat punch. *Proceedings of the Institution of Mechanical Engineers*, 1998, Vol. 212C, pp. 319-327.

9) M.A. Sadowsky, Two-dimensional problems of elasticity theory. *Zeitschrift für angewandte Mathematik und Mechanik,* 1928, Vol. 8, pp. 107–121.

10) J.W. Harding, I.N. Sneddon, The elastic stresses produced by the indentation of the plane surface of a semi-infinite elastic solid by a rigid punch. *Proceedings of the Cambridge Philosophical Society*, 1945, Vol. 41, pp. 16-26.

11) M. Ciavarella, Indentation by nominally flat or conical indenters with rounded corners. *International Journal of Solids and Structures*, 1999, Vol. 36, pp. 4149-4181.

APPENDIX

Here we furnish peak stress values for the following test problems, in order: plane-strain contact patch tests (with matched and mismatched nodes), axisymmetric contact patch tests (with matched and mismatched nodes), plane-strain Hertzian contact, axisymmetric Hertzian contact, plane-strain Steuermann contact, plane-strain flat punch contact, and axisymmetric flat punch contact.

Plane-strain contact patch tests: maximum vertical stress

$\overline{\sigma_z} = -\sigma_z^{\max} / p =$ 1.0000 (exact value from Equation (6))

Matched nodes

$\overline{\sigma_z}$ from surface-to-surface elements with AL, PM options is 1.0000 for all meshes and both 4Q and 8Q host elements.

Table 3a : $\overline{\sigma_z}$ from 4Q elements

Mesh	Contact algorithm		
	AL, PM *	LMP, PLM **	IMC **
C	1.0183	1.0001	1.9508
M	1.0361	1.0003	2.3273
F	1.0694	1.0019	2.7767

***** Node-to-surface ** Either node-to-surface or surface-to-surface

Table 3b : $\overline{\sigma_z}$ from 8Q elements

Mesh	Contact algorithm		
	AL, PM *	LMP, PLM **	IMC **
C	1.3243	1.3189	1.8673
M	1.3238	1.3135	2.2076
F	1.3308	1.3118	2.6285

***** Node-to-surface ** Either node-to-surface or surface-to-surface

Mismatched nodes

Table 4a : $\overline{\sigma_z}$ from surface-to-surface 4Q elements

Mesh	Contact algorithm		
	AL, PM	LMP, PLM *	IMC *
C	1.0425	1.1707	2.1213
M	1.0425	1.1711	2.5183
F	1.0425	1.1719	2.9968

***** Either node-to-surface or surface-to-surface

Table 4b : $\overline{\sigma_z}$ from surface-to-surface 8Q elements

Mesh	Contact algorithm		
	AL, PM	LMP, PLM *	IMC *
C	1.0704	1.3166	1.8791
M	1.0704	1.3127	2.2171
F	1.0704	1.3115	2.6370

***** Either node-to-surface or surface-to-surface

Table 4c : $\overline{\sigma_z}$ from node-to-surface elements

Mesh	Contact algorithm: AL, PM	
	4Q	8Q
C	1.1834	1.3233
M	1.1961	1.3253
F	1.2202	1.3345

Axisymmetric contact patch tests: maximum vertical stress

$\overline{\sigma_z} = -\sigma_z^{\max} / p =$ 1.0000 (exact value from Equation (8))

Matched nodes

Table 5a : $\overline{\sigma_z}$ from surface-to-surface 4Q elements

Mesh	Contact algorithm		
	AL, PM	LMP, PLM *	IMC*
C	1.0023	1.0002	1.8555
M	1.0095	1.0005	2.2052
F	1.0382	1.0015	2.6277

***** Either node-to-surface or surface-to-surface

Table 5b : $\overline{\sigma_z}$ from surface-to-surface 8Q elements

Mesh	Contact algorithm		
	AL, PM	LMP, PLM*	IMC*
C	1.0011	1.3856	1.7733
M	1.0047	1.3431	2.0900
F	1.0192	1.3263	2.4859

***** Either node-to-surface or surface-to-surface

Table 5c : $\overline{\sigma_z}$ from node-to-surface elements

Mesh	Contact algorithm: AL, PM	
	4Q	8Q
C	1.0638	1.4072
M	1.1310	1.3768
F	1.2434	1.3766

Mismatched nodes

Table 6a : $\overline{\sigma_z}$ from surface-to-surface 4Q elements

Mesh	Contact algorithm		
	AL, PM	LMP, PLM*	IMC*
C	1.0506	1.5257	1.9971
M	1.0525	1.5258	2.3731
F	1.0605	1.5260	2.8273

***** Either node-to-surface or surface-to-surface

Table 6b : $\overline{\sigma_z}$ from surface-to-surface 8Q elements

Mesh	Contact algorithm		
	AL, PM	LMP, PLM*	IMC*
C	1.0726	1.3670	1.7837
M	1.0725	1.3361	2.0981
F	1.0724	1.3232	2.4930

***** Either node-to-surface or surface-to-surface

Table 6c : $\overline{\sigma_z}$ from node-to-surface elements

Mesh	Contact algorithm: AL, PM	
	4Q	8Q
C	1.6167	1.3916
M	1.6442	1.3750
F	1.6715	1.3784

Plane-strain Hertzian contact: contact stress

$\overline{\sigma_c} = -\sigma_{z(x=0,z=0)} / p =$ 1.2732 (exact value from Equation (15))

Table 7a : $\overline{\sigma_c}$ from surface-to-surface 4Q elements

Mesh	Contact algorithm		
	AL, PM	LMP, PLM	IMC
C	1.2628	1.3124	1.4499
M	1.2704	1.3114	1.4773
F	1.2737	1.3115	1.7387

Table 7b : $\overline{\sigma_c}$ from node-to-surface 4Q elements

Mesh	Contact algorithm		
	AL, PM	LMP, PLM	IMC
C	1.3453	1.3126	1.4711
M	1.4032	1.3103	1.5592
F	1.4104	1.3138	1.8836

Table 7c : $\overline{\sigma_c}$ from surface-to-surface 8Q elements

Mesh	Contact algorithm		
	AL, PM	LMP, PLM	IMC
C	1.2961	1.3409	1.6313
M	1.2809	1.3183	1.4320
F	1.2761	1.3121	1.4630

Table 7d : $\overline{\sigma_c}$ from node-to-surface 8Q elements

Mesh	Contact algorithm	
	AL, PM	IMC
C	1.3516	1.4842
M	1.3428	1.4475
F	1.3972	1.5929

Note: LMP, PLM have the same results as for surface-to-surface elements

Plane-strain Hertzian contact: horizontal stress

$\overline{\sigma_h} = -\sigma_{x(x=0,z=0)} / p =$ 1.2732 (exact value from Equation (15))

Table 8a : $\overline{\sigma_h}$ from surface-to-surface 4Q elements

Mesh	Contact algorithm		
	AL, PM	LMP, PLM	IMC
C	1.2119	1.3724	2.2229
M	1.2214	1.3787	2.3068
F	1.2241	1.3793	2.7642

Table 8b : $\overline{\sigma_h}$ from node-to-surface 4Q elements

Mesh	Contact algorithm		
	AL, PM	LMP, PLM	IMC
C	1.3724	1.3724	2.2722
M	1.4013	1.3779	2.4498
F	1.4111	1.3818	3.0054

Table 8c : $\overline{\sigma_h}$ from surface-to-surface 8Q elements

Mesh	Contact algorithm		
	AL, PM	LMP, PLM	IMC
C	1.2188	1.3891	2.5058
M	1.2216	1.3804	2.2363
F	1.2237	1.3791	2.3094

Table 8d : $\overline{\sigma_h}$ from node-to-surface 8Q elements

Mesh	Contact algorithm	
	AL, PM	IMC
C	1.3870	2.2846
M	1.3878	2.2983
F	1.4216	2.5463

Note: LMP, PLM have the same results as for surface-to-surface elements

Axisymmetric Hertzian contact: contact stress

$\overline{\sigma_c} = -\sigma_{z(r=0,z=0)} / p =$ 1.5000 (exact value from Equation (22))

Table 9a : $\overline{\sigma_c}$ from surface-to-surface 4Q elements

Mesh	Contact algorithm		
	AL, PM	LMP, PLM	IMC
C	1.1992	1.1510	1.5634
M	1.3930	1.3982	1.4948
F	1.4771	1.4981	1.7299

Table 9b : $\overline{\sigma_c}$ from node-to-surface 4Q elements

Mesh	Contact algorithm		
	AL, PM	LMP, PLM	IMC
C	1.2292	1.1763	1.2144
M	1.4287	1.3824	1.5522
F	1.5169	1.5053	1.9684

Table 9c : $\overline{\sigma_c}$ from surface-to-surface 8Q elements

Mesh	Contact algorithm		
	AL, PM	LMP, PLM	IMC
C	1.8390	1.8403	2.4085
M	1.5280	1.5967	2.2208
F	1.4349	1.5830	1.7335

Table 9d : $\overline{\sigma_c}$ from node-to-surface 8Q elements

Mesh	Contact algorithm		
	AL, PM	LMP, PLM	IMC
C	1.8092	1.8436	2.5281
M	1.5406	1.5254	1.8046
F	1.5751	1.5682	1.7219

Plane-strain Steuermann contact: contact stress

$\overline{\sigma_c} = -\sigma_{z(\max \text{ on } z=0)} / p = 9.9773$ (exact value from Equation (31))

$r_e / b = 1,\ p / E = 1/10^3, \nu = 1/4$

Table 10a : $\overline{\sigma_c}$ from surface-to-surface 4Q elements

Mesh	Contact algorithm		
	AL, PM	LMP, PLM	IMC
C	8.7858	9.3506	28.6163
M	9.3539	9.7120	22.0331
F	9.3394	9.8499	17.1295

Table 10b : $\overline{\sigma_c}$ from node-to-surface 4Q elements

Mesh	Contact algorithm	
	AL, PM	IMC
C	9.0534	24.4481
M	9.3384	19.4696
F	9.0019	15.4069

Note: LMP, PLM have the same results as for surface-to-surface elements

Table 10c : $\overline{\sigma_c}$ from surface-to-surface 8Q elements

Mesh	Contact algorithm		
	AL, PM	LMP, PLM	IMC
C	9.0019	10.3627	38.2454
M	9.3272	10.0533	29.6982
F	9.1102	9.9417	22.3978

Table 10d : $\overline{\sigma_c}$ from node-to-surface 8Q elements

Mesh	Contact algorithm	
	AL, PM	IMC
C	10.2553	31.9683
M	9.9544	24.3150
F	9.6914	18.6113

Note: LMP, PLM have the same results as for surface-to-surface elements

Plane-strain Steuermann contact: contact stress

$\overline{\sigma_c} = -\sigma_{z\,(\max \text{ on } z=0)} / p = 10.9571$ (exact value from Equation (31))

$r_e / b = 1/3$, $p / E = 1/10^3$, $\nu = 1/4$

Table 11a : $\overline{\sigma_c}$ from surface-to-surface 4Q elements

Mesh	Contact algorithm		
	AL, PM	LMP, PLM	IMC
C	9.0103	9.9830	33.5897
M	9.4570	10.6177	29.5660
F	9.5320	10.8319	22.8549

Table 11b : $\overline{\sigma_c}$ from node-to-surface 4Q elements

Mesh	Contact algorithm	
	AL, PM	IMC
C	9.9844	33.5897
M	9.7308	25.6857
F	9.1922	20.1155

Note: LMP, PLM have the same results as for surface-to-surface elements

Table 11c : $\overline{\sigma_c}$ from surface-to-surface 8Q elements

Mesh	Contact algorithm		
	AL, PM	LMP, PLM	IMC
C	9.0061	11.3794	56.5126
M	9.2091	11.0536	38.4305
F	9.0159	10.9214	29.6991

Table 11d : $\overline{\sigma_c}$ from node-to-surface 8Q elements

Mesh	Contact algorithm	
	AL, PM	IMC
C	11.3789	43.4274
M	11.0531	32.2514
F	10.9205	24.5035

Note: LMP, PLM have the same results as for surface-to-surface elements

Plane-strain Steuermann contact: contact stress

$\overline{\sigma_c} = -\sigma_{z\,(\max \text{ on } z=0)} / p = 13.1753$ (exact value from Equation (31))

$r_e / b = 1/7$, $p/E = 1/10^3$, $\nu = 1/4$

Table 12a : $\overline{\sigma_c}$ from surface-to-surface 4Q elements

Mesh	Contact algorithm		
	AL, PM	LMP, PLM	IMC
C	10.1611	11.8341	53.2126
M	10.4569	12.5602	40.2460
F	10.5445	12.7074	30.7857

Table 12b : $\overline{\sigma_c}$ from node-to-surface 4Q elements

Mesh	Contact algorithm		
	AL, PM	LMP, PLM	IMC
C	11.2988	11.8327	46.1147
M	11.3911	12.5606	34.6083
F	10.6425	12.7074	26.9414

Table 12c : $\overline{\sigma_c}$ from surface-to-surface 8Q elements

Mesh	Contact algorithm		
	AL, PM	LMP, PLM	IMC
C	9.8124	13.5089	70.4673
M	9.9966	13.0697	54.1219
F	9.7533	12.9042	40.4832

Table 12d : $\overline{\sigma_c}$ from node-to-surface 8Q elements

Mesh	Contact algorithm	
	AL, PM	IMC
C	13.2024	58.6219
M	12.6680	43.7157
F	12.0516	33.0778

Note: LMP, PLM have the same results as for surface-to-surface elements

Plane-strain flat punch: contact stress

$\overline{\sigma_c}^* = -\sigma_{z\,(x=a,z=0)} / p \to \infty$ (analytical value from Equation (39))

Table 13a : $\overline{\sigma_c}^*$ from surface-to-surface 4Q elements

Mesh	Contact algorithm		
	AL, PM	LMP, PLM	IMC
C	2.1318	2.2699	1.9885
M	3.0164	3.2185	2.7008
F	4.2661	4.5574	3.6348

Table 13b : $\overline{\sigma_c}^*$ from node-to-surface 4Q elements

Mesh	Contact algorithm	
	AL, PM	IMC
C	2.2135	1.9885
M	3.0526	2.7008
F	4.1057	3.6348

Note: LMP, PLM have the same results as for surface-to-surface elements

Table 13c : $\overline{\sigma_c}^*$ from surface-to-surface 8Q elements

Mesh	Contact algorithm		
	AL, PM	LMP, PLM	IMC
C	1.7360	1.7772	1.7844
M	2.4374	2.5722	2.4258
F	3.4344	3.7990	3.2666

Table 13d : $\overline{\sigma_c}^*$ from node-to-surface 8Q elements

Mesh	Contact algorithm	
	AL, PM	IMC
C	1.7677	1.7844
M	2.4729	2.4258
F	3.4127	3.2666

Note: LMP, PLM have the same results as for surface-to-surface elements

Axisymmetric flat punch: contact stress

$\overline{\sigma_c}^* = -\sigma_{z\,(r=a,z=0)} / p \to \infty$ (analytical value from Equation (45))

Table 14a : $\overline{\sigma_c}^*$ from surface-to-surface 4Q elements

Mesh	Contact algorithm		
	AL, PM	LMP, PLM	IMC
C	1.6408	2.8492	1.5882
M	2.3472	4.0875	2.2178
F	3.3380	5.8223	3.0487

Table 14b : $\overline{\sigma_c}^*$ from node-to-surface 4Q elements

Mesh	Contact algorithm	
	AL, PM	IMC
C	1.6102	1.5882
M	2.1432	2.2178
F	2.7051	3.0487

Note: LMP, PLM have the same results as for surface-to-surface elements

Table 14c : $\overline{\sigma_c}^*$ from surface-to-surface 8Q elements

Mesh	Contact algorithm		
	AL, PM	LMP, PLM	IMC
C	1.3208	1.3373	1.4152
M	1.8836	1.9569	1.9850
F	2.6778	2.8110	2.7352

Table 14d : $\overline{\sigma_c}^*$ from node-to-surface 8Q elements

Mesh	Contact algorithm		
	AL, PM	LMP, PLM	IMC
C	1.2979	1.3373	1.4152
M	1.8076	1.9411	1.9850
F	2.4080	2.8214	2.7352

VITA

Serhan Sezer was born on May 6, 1980, in Herisau, Switzerland. He received his high school diploma from Bursa Erkek Lisesi in Bursa, Turkey, in June of 1997. Next, he obtained the degree of Bachelor of Science in Mechanical Engineering in July of 2002 from Yildiz Technical University in Istanbul, Turkey. Serhan then attended Louisiana State University Graduate School to pursue a Master of Science Degree in Mechanical Engineering in August of 2003.